

# Observation of Ferroelectricity in the Kitaev Paramagnetic State of $\alpha$ -RuCl<sub>3</sub>

Xinrun Mi,<sup>1,\*</sup> De Hou<sup>\*,2,3</sup> Xiao Wang<sup>\*,4</sup> Caixing Liu,<sup>2</sup> Zijian Xiong,<sup>1</sup> Han Li,<sup>5</sup> Aifeng Wang,<sup>1</sup> Yisheng Chai,<sup>1</sup> Yang Qi,<sup>6</sup> Wei Li,<sup>7</sup> Xiaoyuan Zhou,<sup>1</sup> Yixi Su,<sup>4</sup> D. I. Khomskii,<sup>8</sup> Mingquan He,<sup>1,†</sup> Zhigao Sheng,<sup>2,‡</sup> and Young Sun<sup>1,§</sup>

<sup>1</sup>College of Physics & Center of Quantum Materials and Devices, Chongqing University, Chongqing 401331, China

<sup>2</sup>Anhui Key Laboratory of Condensed Matter Physics at Extreme Conditions,  
High Magnetic Field Laboratory, HFIPS, Anhui,  
Chinese Academy of Sciences, Shushanhu Road 350, Hefei, 230031 China

<sup>3</sup>University of Science and Technology of China, Hefei 230026, China

<sup>4</sup>Jülich Centre for Neutron Science (JCNS) at Heinz Maier-Leibnitz Zentrum (MLZ),  
Forschungszentrum Jülich GmbH, Lichtenbergstr. 1, D-85747 Garching, Germany

<sup>5</sup>School of Physics, Beihang University, Beijing 100191, China

<sup>6</sup>State Key Laboratory of Surface Physics & Department of Physics, Fudan University, 200433, Shanghai, China

<sup>7</sup>Institute of Theoretical Physics, Chinese Academy of Sciences, Beijing 100190, China

<sup>8</sup>II. Physikalisches Institut, Universität zu Köln, D-50937 Köln, Germany

(Dated: May 20, 2022)

The spin-orbit assisted Mott insulator  $\alpha$ -RuCl<sub>3</sub> is a prime candidate for material realization of the Kitaev quantum spin liquid. While little attention has been paid to charge degrees of freedom, charge effects, such as electric polarization, may arise in this system, which could possibly allow electrical access to low-energy excitations of quantum spin liquids. Here, we demonstrate ferroelectricity in  $\alpha$ -RuCl<sub>3</sub>, by means of pyroelectric, second harmonic generation and specific heat measurements. The electric polarization and second harmonic generation signal develop substantially in the Kitaev paramagnetic state when short-range spin correlations come into play. The electric polarization appears mainly within the honeycomb plane and responds weakly to external magnetic fields. Virtual hopping induced charge redistribution, together with moderate in-plane distortions, are likely responsible for the establishment of electric polarization, which gets boosted by short-range spin correlations. Our results emphasize the importance of charge degrees of freedom in  $\alpha$ -RuCl<sub>3</sub>, which establish a novel platform to investigate charge effects in Kitaev materials, and enrich the intriguing Kitaev physics.

The intricate interplay of spin, charge, orbital, and lattice degrees of freedom in Mott insulators often gives rise to a broad variety of quantum phases of matter, such as high-temperature superconductivity, frustrated magnetism, and nontrivial topological orders [1–3]. Of particular interests are spin-orbit assisted Mott insulators, including  $\alpha$ -RuCl<sub>3</sub>, A<sub>2</sub>IrO<sub>3</sub> (A = Li, Na), which represent prime material playgrounds to pursue the long-sought Kitaev quantum spin liquid (QSL) [4–6]. The Kitaev QSL is characterised by frustrated bond-dependent Kitaev interactions, which can host emergent  $\mathbb{Z}_2$ -fluxes and Majorana fermion excitations that could be promising ingredients towards topological quantum computing [7, 8]. Exploration of QSL excitations in Mott insulating Kitaev materials, both in magnetic and charge channels, is of great fundamental and technical importance [9, 10].

Compared with intensive studies in the spin channel, charge degrees of freedom are often overlooked in Kitaev materials. Due to strong on-site Coulomb repulsion, electronic charges are largely localized in the Mott insulating state. The ground state and low-energy excitations, thus, are typically treated by the remaining spin degrees of freedom. Nevertheless, electrons are allowed to virtually

visit neighboring sites, which actually is the key ingredient to mediate exchange interactions in the spin channel. Theoretically, such virtual hopping of electrons can give rise to various intriguing charge effects, such as fractional charges, spontaneous orbital currents, and electric polarization [11–18]. To realize these charge effects, geometrically frustrated lattices are generally required in the framework of the single-band Hubbard model [14, 15]. On the other hand, similar effects can survive in bipartite Kitaev materials with multiorbital characters, due to the interplay of spin-orbit coupling, crystal field distortion, and Hund’s coupling [19, 20]. This scenario is likely realized in the spin-orbit entangled Kitaev material  $\alpha$ -RuCl<sub>3</sub> [19, 20], which has sizable electronic dipole contributions to the observed subgap optical conductivity [21–25]. Even more interesting in this respect is the possibility to access, and even manipulate low-energy QSL excitations electrically via these charge effects [9, 10, 26–28]. Experimental identification of charge effects in QSL candidates would be essential towards QSL-based applications.

Here, we have discovered ferroelectricity in  $\alpha$ -RuCl<sub>3</sub>, which establishes a prominent platform for searching charge effects in Kitaev materials. The 4d transition-metal binary halide  $\alpha$ -RuCl<sub>3</sub> is a spin-orbit assisted Mott insulator with moderate electronic correlations ( $U \sim 2$  eV) and sizable nearest-neighbor hopping ( $t \sim 100$  meV) [19, 20, 29–33]. Finite values of  $t/U$  and wide-spread  $d$ -orbitals are advantageous for the development of charge

\* These authors contributed equally to this work.

† [mingquan.he@cqu.edu.cn](mailto:mingquan.he@cqu.edu.cn)

‡ [zhigaosheng@hml.ac.cn](mailto:zhigaosheng@hml.ac.cn)

§ [youngsun@cqu.edu.cn](mailto:youngsun@cqu.edu.cn)

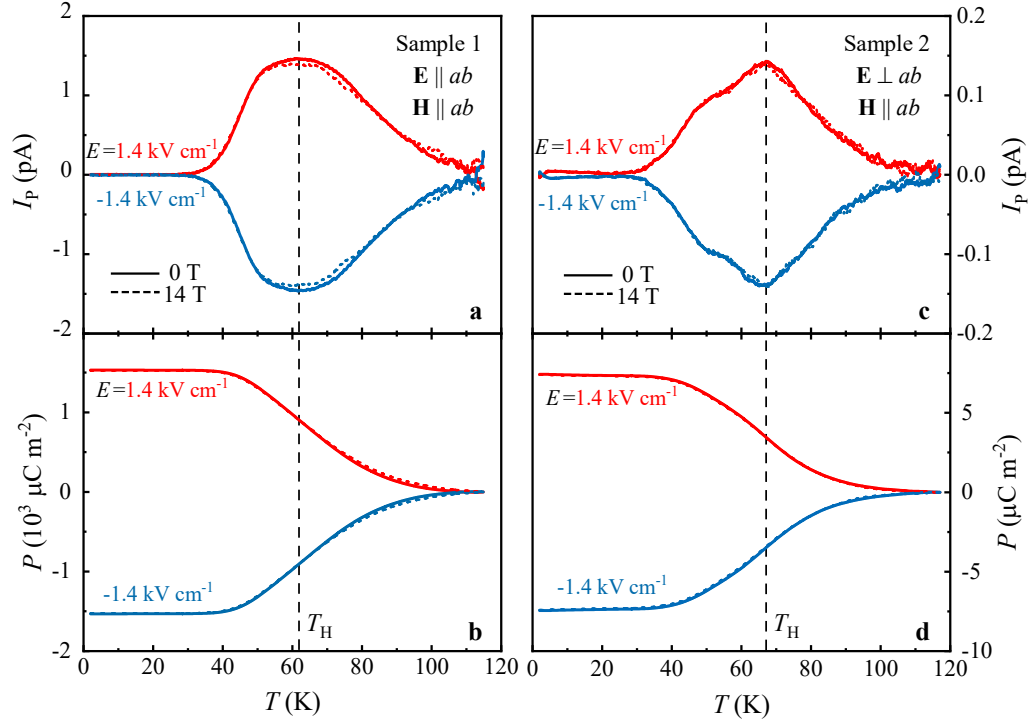


**Figure 1. Temperature evolution of electric polarization.** **a,b**, The pyroelectric current ( $I_P$ ) and the integrated electric polarization ( $P$ ) of sample 1 using an  $\mathbf{E} \parallel ab$  poling configuration. **c,d**, Same measurements with those of **a,b** for sample 2, which were performed with an out-of-plane  $\mathbf{E} \perp ab$  poling geometry. For both samples,  $I_P$  peaks around  $T_H \sim 60$  K (vertical dash lines), which respond weakly to in-plane magnetic fields up to 14 T.

fluctuations. This compound is a van der Waals layered material, and each layer is formed by edge-sharing  $\text{RuCl}_6$  octahedra. The presence of octahedra crystal fields, together with strong spin-orbit coupling ( $\lambda \sim 150$  meV), lead to an effective  $J = 1/2$  ground state for the  $4d^5$  ( $\text{Ru}^{3+}$ ) configuration. The Ru atoms form a nearly ideal honeycomb lattice within the  $ab$  plane, which is in close proximity to the Kitaev QSL [34–41]. Although finite non-Kitaev interactions drive  $\text{RuCl}_3$  into a zigzag anti-ferromagnetic (AFM) phase below  $T_N \sim 7$  K, the Kitaev fluctuations and fractional excitations survive up to  $T_H \sim 70 - 100$  K in the Kitaev paramagnetic state [39–41].

To investigate the charge effects, we start with pyroelectric experiments, and the results are presented in Fig. 1. Two typical single crystals, sample 1 and sample 2, were studied with poling electric fields applied in-plane ( $\mathbf{E} \parallel ab$ ) and out-of-plane ( $\mathbf{E} \perp ab$ ), respectively. Similar results are found in other samples, which can be found in Supplementary Material. A highly hysteretic structure transition typically occurs around 50 K and 170 K upon cooling and heating [41–45]. To avoid the impacts of structure transition, all measurements in this study were performed upon warming. A clear but broad peak centered around  $T_H \sim 60$  K is seen in both samples, as shown in Figs. 1a,c. More importantly, the sign of the observed pyroelectric current is switchable by reversing

the direction of poling electric fields. These findings imply the existence of ferroelectricity in  $\text{RuCl}_3$ . Application of in-plane magnetic fields, on the other hand, has minimal effects on the pyroelectric current for both samples. Negligible response is also found by applying out-of-plane magnetic fields (see Supplementary Material). Note that the magnitude of the pyroelectric current observed in sample 1 using the  $\mathbf{E} \parallel ab$  poling configuration, is one order of magnitude larger than that in sample 2 with  $\mathbf{E} \perp ab$ . In Figs. 1e,f, by integrating the pyroelectric current out, the electric polarization  $P$  is directly compared for these two samples. Sizable polarization reaching  $P = 1.5 \times 10^3 \mu\text{C m}^{-2}$  is found for sample 1 below 40 K, which is three orders of magnitude larger than that of sample 2. The polarization is therefore mainly developing within the honeycomb plane. Instead of a well defined phase transition, the polarization picks up its value gradually, showing crossover-like behaviour. This suggests that the dipole-dipole interactions are only short-ranged, leading to a relaxor ferroelectric behaviour, which is also evidenced by highly frequency dependent dielectric constant (see Supplementary Material).

The observation of ferroelectricity is necessarily associated with inversion-symmetry-breaking. Lack of inversion center produces nonlinear optical response, which can be captured nicely by second harmonic generation (SHG) techniques [46, 47]. We present the SHG results

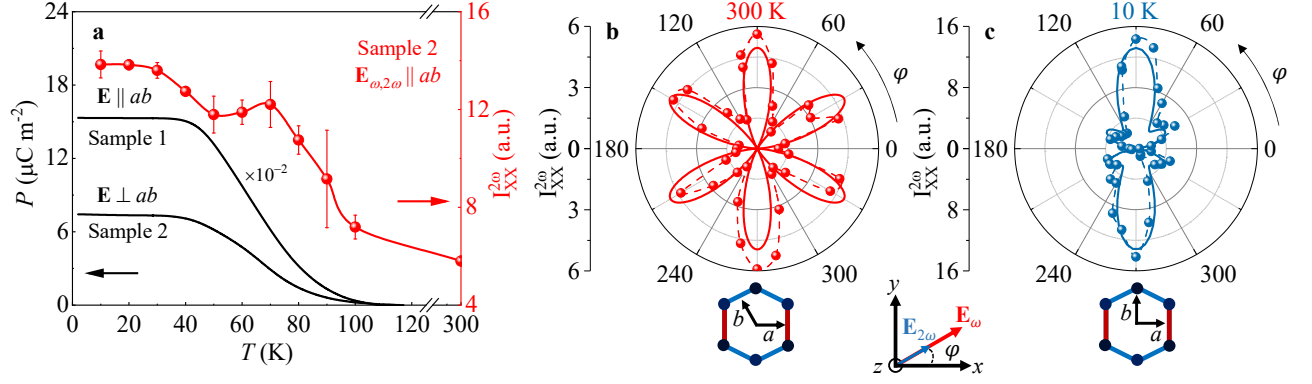


**Figure 2. Second harmonic generation (SHG).** **a**, Temperature dependence of SHG intensity ( $I_{XX}^{2\omega}$ , red spheres) measured for sample 2 using a normal incidence geometry ( $\mathbf{E}_{\omega, 2\omega} \parallel ab$ ). The fundamental and second harmonic beams were linearly co-polarized. Electric polarization (black lines) obtained in pyroelectric experiments is also presented for comparison. **b,c**, Polar plots of SHG intensity recorded at 300 K and 10 K. The lab coordinates are denoted as  $(x, y, z)$  and the  $\varphi = 0$  direction points perpendicular to the Ru-Ru bounds. Solid lines are theoretical fitting using  $D_3$  and  $C_2$  symmetries for data obtained at 300 K and 10 K, respectively. Dashed lines are guide to the eye. Bottom panels in **b,c** illustrate the Ru lattice in trigonal and monoclinic representations (red bonds differ from blue bonds slightly).

obtained for sample 2 in Fig. 2 using a normal incidence geometry, which was not poled by an external electric field. Here, we focus on a linearly co-polarized configuration (XX) of fundamental and second harmonic beams. Data collected using a linearly cross-polarized (XY) geometry can be found in Supplementary Material. As shown in Fig. 2a, sizable SHG signal (red spheres) is found below  $T_H$ , which persists up to room temperature with significantly reduced intensity. The SHG signal only varies slightly at low temperatures below  $T_H$ , whereas further warming leads to rapid loss of intensity. Negligible variations are again recovered above 100 K. When compared directly with the polarization results (black lines in Fig. 2a), one readily finds that the drastic changes of SHG in the vicinity of  $T_H$  track nicely with the evolution of electric polarization. In the crossover region (50 K  $\sim$  90 K), we note that error bars of the SHG signal are significantly enhanced, compared with other temperatures. Moreover, the illuminated spot of the sample surface became greenish when passing through the crossover interval (see Supplementary Material). These effects again point to fluctuating, short-ranged dipole correlations, which also cause rapid change in dielectric properties seen by SHG. The development of ferroelectricity near  $T_H$  is therefore firmly supported by the SHG findings.

The appearance of SH response at room temperature put strong constraints on the crystal space group. Due to the nature of van der Waals inter-layer coupling, a variety of crystal structures have been reported, including trigonal  $P3_112$  [36, 48, 49], monoclinic  $C2/m$  [50–52], and rhombohedral  $R\bar{3}$  [43, 53, 54], depending on the inter-layer stacking details. A switching from the high-temperature  $C2/m$  polytype to the low-temperature  $R\bar{3}$  phase (or from  $P3_1$  to  $C2/m$  [49]) at the first-order structure transition has been suggested [43, 54]. Among these

polymorphs, only the  $P3_112$  space group lacks inversion symmetry. The sizable SHG response at 300 K, likely points to a high-temperature  $P3_112$  polytype for the samples studied here.

The point group symmetry can be further explored by presenting polar plots of SHG signal, as shown in Figs. 2b,c. Here, the polarization directions of fundamental and excited detection beams were rotated simultaneously within the sample  $ab$  plane. The  $\varphi = 0$  direction is perpendicular to the Ru-Ru bounds. As expected for the  $P3_112$  family, a threefold rotational symmetry is clearly identified at 300 K, which can be well fitted using the  $D_3$  symmetry (solid line in Fig. 2b, see details in Supplementary Material). Slight deviations from the ideal  $D_3$  symmetry suggest minor distortions of the honeycomb layer, in a way that one type of bonds (red links in the bottom panels of Figs. 2b,c) are slightly longer than other two types (blue bonds) by  $\sim 0.2\%$  [22, 49, 51, 54, 55]. This in-plane distortion turns out to be essential for the establishment of electric polarization in such a bipartite lattice, as we will discuss shortly. At low temperatures, the rotational symmetry is reduced to twofold. The data are nicely described by the  $C_2$  symmetry with the twofold axis directed along the  $b$  direction (see Fig. 2c). More plots captured at other temperatures are shown in Supplementary Material. Similar  $C_2$  symmetric properties in the low-temperature phase have also been reported by anisotropic susceptibility measurements [56]. This symmetry reduction from trigonal ( $D_3$ ) to monoclinic ( $C_2$ ) is likely resulted from the first-order structure transition, agreeing well with earlier neutron experiments [49].

To further unveil the origin of the observed ferroelectricity, we compare the pyroelectric current and magnetic specific heat in Fig. 3. The magnetic specific heat  $C_M = C_{\text{total}} - C_{\text{ph}}$  is obtained by subtracting the phonon contribution  $C_{\text{ph}}$  from the measured total specific heat

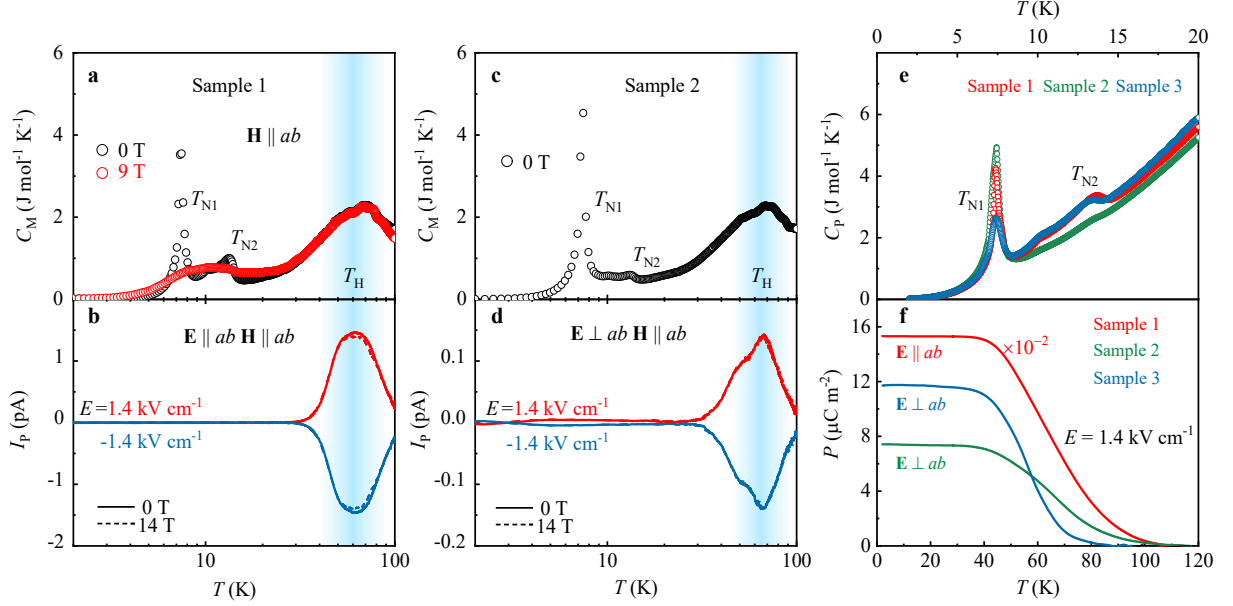


**Figure 3. Correlation between electric polarization and short-range spin correlations.** Comparison of magnetic specific heat ( $C_M$ , **a,c**) and pyroelectric current (**b,d**) of sample 1 and sample 2. The pyroelectric current peak appears concomitantly with the hump in specific heat around  $T_H$ , suggesting intimate coupling between electric polarization and short-range spin correlations. **e**, Specific heat measured near the AFM transitions, which characterizes different degrees of stacking faults for three samples. **f**, Electric polarization of the corresponding samples, which only depends weakly on stacking faults. The polarization of sample 1 is scaled by a factor of  $10^{-2}$  for better comparison.

$C_{\text{total}}$ . The phonon background is estimated from an isostructural non-magnetic material  $\text{RhCl}_3$  following S. Widmann *et al.* [41] (see Supplementary Material for more details). As seen in Figs. 3a,c, a broad hump appears clearly in  $C_M$  around  $T_H$ , agreeing well with former studies [40, 41]. This high-temperature peak is very likely correlated with entropy release of Majorana fermion excitations in the Kitaev framework [40, 41, 57–61]. Signatures of fractional excitations emerging near  $T_H$  have also been evidenced by various other techniques [34–41]. It becomes clear that short-range spin correlations start to develop in the vicinity of  $T_H$ , regardless of their microscopic origin. Interestingly, the pyroelectric current peak occurs concomitantly with the broad hump in specific heat for both samples with different poling directions. The evolution of electric polarization certainly are correlated with short-range spin correlations.

In addition to the high-temperature peak, we note that there are two other anomalies appearing in specific heat at  $T_{N1} \sim 7$  K and  $T_{N2} \sim 14$  K for both samples, which are signatures of long-range ordered zigzag AFM transitions. Appearance of multiple transitions suggests the existence of stacking faults. It has been suggested that an  $ABC$  inter-layer stacking gives rise to the transition at  $T_{N1}$ , whereas an  $ABAB$  stacking leads to the transition at  $T_{N2}$  [50]. The magnetic orders can be suppressed by an in-plane magnetic field of 9 T, as shown in Fig. 3a. However, the high-temperature peak in  $C_M$  remains nearly intact in the presence of magnetic fields, as also

found by S. Widmann *et al.* [41]. Similarly, the pyroelectric current also respond weakly to external magnetic fields, as shown in Figs. 3b,d. This again suggests that spin correlations are short-ranged at an energy scale of  $T_H$ .

Formation of stacking faults can break the inversion symmetry locally at  $ABAB$  and  $ABC$  stacking interfaces, which can give rise to local electric polarization [45]. To explore the influence of stacking faults, the polarization measured for three samples with different degrees of stacking faults are compared in Fig. 3f. Sample 2 has minimal stacking faults as the AFM transition is dominated by a sharp peak in specific heat at  $T_{N1}$  (see Fig. 3e). On the other hand, sizable stacking faults are found in sample 3, which shows suppressed transition at  $T_{N1}$  and enhanced transition at  $T_{N2}$ , compared with other two samples. And sample 1 lies somewhere in between. As shown in Figs. 3e,f, we find no clear connection between stacking faults and the magnitude of polarization. The largest polarization is found in sample 1 using a poling configuration of  $\mathbf{E} \parallel ab$ . Although sample 2 and sample 3 possess different degrees of stacking faults, they share similar magnitude of polarization in an  $\mathbf{E} \perp ab$  geometry, which is orders magnitude smaller than that of sample 1. Therefore, the polarization depends strongly on poling directions, and not on stacking faults. In addition, stacking faults only break the inversion symmetry perpendicular to the  $ab$  plane, which would unlikely produce large in-plane polarization. The fact that sample

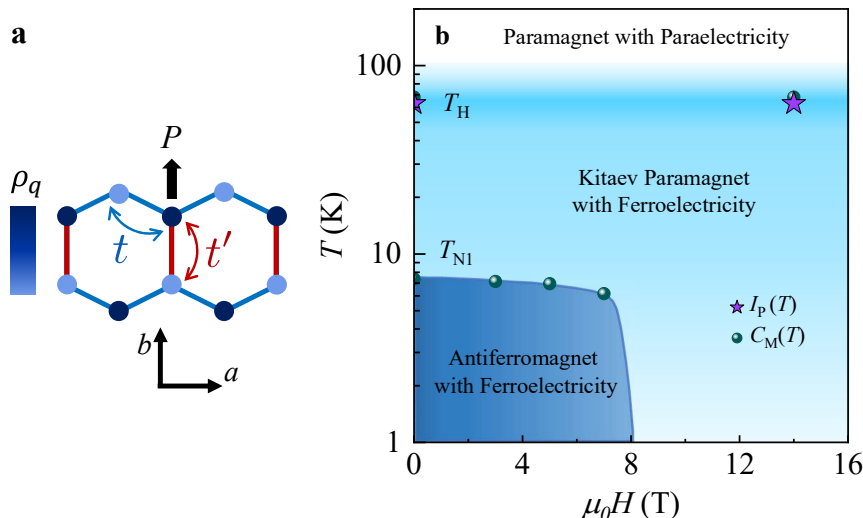


**Figure 4. Phase diagram.** **a**, Schematic illustration of charge modulation induced electric polarization in  $\text{RuCl}_3$ . Charge density ( $\rho_q$ ) distributes inhomogeneously on a distorted lattice due to anisotropic hopping ( $t \neq t'$ ) along nearest neighbouring bonds, forming a local trigonal charge order, which gives rise to electric polarization along the  $b$  direction. **b**, Phase diagram of  $\text{RuCl}_3$ . The ferroelectricity emerges concomitantly with the Kitaev paramagnetic state. Solid green spheres and purple stars are extracted from the temperature dependence of specific heat  $C_M(T)$  and pyroelectric current  $I_P(T)$ , respectively.

3 has slightly larger polarization than that in sample 2, suggests moderate contributions of stacking faults to the out-of-plane polarization.

As discussed above, external magnetic field can hardly affect the observed ferroelectricity, which is reminiscent of the charge-order-driven ferroelectricity found in molecular dimer Mott insulators [62–64]. Trigonal and dimer-like charge orders have indeed been visualized in  $\text{RuCl}_3$  by scanning tunnelling microscopy (STM) [49], which is one possible driving force of the ferroelectricity observed here. Unlike the spin-driven ferroelectricity, the well separated crossover-like ferroelectric and long-range AFM transitions in  $\text{RuCl}_3$  also favor an electronic origin. For the  $4d^5$  configuration of  $\text{Ru}^{+3}$  valence state, one hole per site is expected without any polarization. However, the average charge density per site ( $\rho_q$ ) can deviate from 1 due to virtual charge hopping among neighbouring sites [14, 15]. As shown in Fig. 4a, to mimic the case of  $\text{RuCl}_3$ , we consider a distorted two-dimensional honeycomb lattice, i.e., bonds along the  $b$  direction differ slightly from other two types (see also Fig. 2). The bond anisotropy leads to anisotropic hopping processes ( $t \neq t'$ ), which likely produce the charge orders detected by previous STM measurements even at room temperature [49]. The inversion symmetry is broken by this kind of site- and bond-centered charge ordering [65, 66], which gives in-plane electric polarization locally along the  $b$ -axis (see Fig. 4a). Still, spin correlations can also contribute to the appearance of electric dipoles and to the ferroelectricity [14, 15]. At high temperatures, electric dipole-dipole correlations are hindered by thermal fluctuations, and the system is in the paraelectric state. As indicated in the specific heat measurements, virtual hop-

ping mediated short-range spin correlations are built up near  $T_H$ . This could also enhance the dipole-dipole interactions (and/or vice versa) in the electric channel via strong spin-orbit coupling and magnetoelastic coupling. Inelastic X-ray scattering experiments have revealed substantial phonon softening below  $\sim 100$  K, indicating sizable spin-phonon coupling at this temperature scale [67]. Due to the short-ranged nature of the dipole-dipole interactions, a crossover-like behaviour appears in accordance with our observations (see Figs. 1,2).

Local charge imbalance induced polarization is also possible even in the pure Kitaev scenario [10, 19, 20], which likely explains the subgap optical conductivity found by terahertz spectroscopy experiments [21–25]. There, the electric polarization arises at the second order of hopping amplitude in the presence of finite trigonal distortion, Hund’s coupling and strong spin-orbit coupling. The presence of magnetoelectric coupling could further produce a Majorana-Fermi surface [28] in the Kitaev QSL. Moreover, as shown by R. G. Pereira *et al.* [10], finite charge modulations and electric polarization can arise around  $\mathbb{Z}_2$  vortices, allowing electrical control of gauge fluxes and fractional spin excitations [10]. However, one may expect cross-tuning effects of electric (magnetic) properties using magnetic (electric) fields, which are not evident in our experiments. Nevertheless, this possibility can not be completely ruled out, since extremely large electric fields ( $E \sim 10^7$  V m $^{-1}$ ) and sufficiently low temperatures ( $\ll 1$  K) may be required to see sizable cross-tuning effects [28]. Further studies are necessary to extract the interplay of electric polarization and low-energy spin excitations.

Finally, we arrive at the phase diagram of  $\alpha\text{-RuCl}_3$ ,



both in the magnetic and electric channels, as shown in Fig. 4b. At high temperatures well above  $T_H$ , spins and electric dipoles are not correlated, the system is at a conventional paramagnetic state and a paraelectric phase. Short-range spin correlations, possibly Kitaev-like, build up near  $T_H$ , which drive  $\alpha$ - $\text{RuCl}_3$  into the Kitaev paramagnetic state at lower temperatures. Concomitantly, short-range dipole-dipole interactions are established, leading to relaxor-like ferroelectricity. This ferroelectric state persists well inside the long-range AFM phase, and survives in the field-induced magnetically disordered state above  $\sim 8$  T.

In summary, we have discovered ferroelectricity in the spin-orbit assisted Mott insulating Kitaev material  $\alpha$ - $\text{RuCl}_3$ . Virtual hopping induced charge fluctuations and moderate in-plane distortions, are key ingredients to promote electric polarization. Our findings suggest that  $\alpha$ - $\text{RuCl}_3$  is a unique system to investigate charge effects in Kitaev materials, and call for further investigations to track down the interplay of electric polarization and novel fractional spin excitations.

## METHODS

**Crystal growth** High-quality single crystalline  $\alpha$ - $\text{RuCl}_3$  samples were grown in a two-zone furnace using the chemical vapour transport method [45]. Commercial  $\text{RuCl}_3$  powder (Furuya metal) was firstly sealed in a silica ampule, which was subsequently inserted into a two-zone furnace. The source and sink temperatures were set to 790 °C and 710 °C, respectively. Single crystals of  $\alpha$ - $\text{RuCl}_3$  were obtained as black shiny plates at the sink end after 5 days.

**Pyroelectric measurement** Two typical types of samples were chosen for pyroelectric measurements. Sample 1 and sample 4 (see Supplementary Material) are relatively thick crystals with typical dimension of  $5 \times 3 \times 0.6$  mm<sup>3</sup>. These two samples were cut into rectangular cuboids with the largest faces perpendicular to the honeycomb layer, so that an  $\mathbf{E} \parallel ab$  poling configuration was adopted. The other type of samples, i.e., sample 2 and sample 3, are thin plates with the widest planes being the  $ab$  plane (typical dimension:  $5 \times 5 \times 0.05$  mm<sup>3</sup>). And an  $\mathbf{E} \perp ab$  poling geometry was used for sample 2 and sample 3. Thin layer of Au (50 nm) was sputtered on the corresponding sample surfaces to serve as contact electrodes for the pyroelectric measurements. Background current was measured by a Keithley 6517B electrometer upon heating ( $3 \text{ K min}^{-1}$ ) after cooling the samples down to 2 K in zero electric field. Subsequently, poling electric fields were applied at 80 K using the Keithley 6517B and the samples were then cooled down in electric fields down to 2 K. The pyroelectric current was finally recorded using the Keithley 6517B upon warming ( $3 \text{ K min}^{-1}$ ) in zero electric field after the electrodes were shortened for 20 min at 2 K. The net pyroelectric current was evaluated by subtracting the background current from the

measured total pyroelectric current. The electric polarization was obtained by integrating the net pyroelectric current. The pyroelectric measurements were carried out in a commercial cryostat (Oxford Instruments, 14 T).

**Second-harmonic generation (SHG)** The SHG measurements were conducted in a low-vibration optical cryostat (ARS, CS204SF-FMX-20) with a base temperature of 10 K. Femtosecond fundamental beams (800 nm) were generated from a Ti: sapphire laser (100 fs, 84 MHz). A normal incidence geometry was adopted, and the probing electric fields of light were directed within the  $ab$  plane of  $\text{RuCl}_3$  samples. The SHG signal was collected using two configurations, XX and XY, in which the fundamental light and the outgoing beam were co- and cross-polarized, respectively. Samples were cleaved *in-situ* before SHG experiments.

**Heat capacity experiment** The specific heat  $C_P$  experiments were performed in a Physical Property Measurement System (Quantum Design Dynacool, 9 T) using the conventional relaxation method from 2 K to 100 K upon warming. The lattice contribution was estimated by the specific heat of a non-magnetic isostructural compound  $\text{RhCl}_3$  using the data reported by S. Widmann *et al.* [41] (see Supplementary Material for more details).

## ACKNOWLEDGMENTS

We thank Long Zhang, Yuan Li and Xuefeng Zhang for stimulating discussions. We thank Guiwen Wang and Yan Liu at the Analytical and Testing Center of Chongqing University for technical support. This work has been supported by National Natural Science Foundation of China (Grant Nos. 11904040, 12047564, 51725104), Chongqing Research Program of Basic Research and Frontier Technology, China (Grant No. cstc2020jcyj-msxmX0263). The work of D. I. Khomskii was funded by the Deutsche Forschungsgemeinschaft (DFG, German Research Foundation) - Project number 277146847 - CRC 1238. Y. Chai acknowledges the support by National Natural Science Foundation of China (Grant Nos. 11674384, 11974065). A. Wang acknowledges the support by National Natural Science Foundation of China (Grant No. 12004056). A portion of this work was performed at the Anhui Laboratory of High Magnetic Field.

## AUTHOR CONTRIBUTIONS

M. H. and Y. S. initiated and supervised this study. X. M. performed the pyroelectric, specific heat experiments with support from Y. C., A. W. Single crystals were prepared and provided by X. W. and Yi. S. And D. H., C. L., Z. S. carried out the second harmonic generation experiments. Z. X., H. L., Y. Q., W. L. and D. I. K. inspired the theoretical interpretations. X. M., D. H., Y. C., Z. S., M. H. and Y. S. prepared the manuscript with

contributions from all other authors.

## COMPETING INTERESTS

The authors declare no competing financial interest.

## ADDITIONAL INFORMATION

More experimental data can be found in Supplementary Material.

- 
- [1] M. Imada, A. Fujimori, and Y. Tokura, *Rev. Mod. Phys.* **70**, 1039 (1998).
  - [2] W. Witczak-Krempa, G. Chen, Y. B. Kim, and L. Balents, *Annu. Rev. Condens. Matter Phys.* **5**, 57 (2014).
  - [3] D. I. Khomskii, *Transition Metal Compounds* (Cambridge University Press, 2014).
  - [4] G. Jackeli and G. Khaliullin, *Phys. Rev. Lett.* **102**, 017205 (2009).
  - [5] L. Savary and L. Balents, *Rep. Prog. Phys.* **80**, 016502 (2016).
  - [6] C. Broholm, R. J. Cava, S. A. Kivelson, D. G. Nocera, M. R. Norman, and T. Senthil, *Science* **367**, eaay0668 (2020).
  - [7] A. Kitaev, *Ann. Phys.* **321**, 2 (2006).
  - [8] C. Nayak, S. H. Simon, A. Stern, M. Freedman, and S. Das Sarma, *Rev. Mod. Phys.* **80**, 1083 (2008).
  - [9] E. J. König, M. T. Randeria, and B. Jäck, *Phys. Rev. Lett.* **125**, 267206 (2020).
  - [10] R. G. Pereira and R. Egger, *Phys. Rev. Lett.* **125**, 227202 (2020).
  - [11] P. Fulde, K. Penc, and N. Shannon, *Annalen der Physik* **11**, 892 (2002).
  - [12] E. Runge and P. Fulde, *Phys. Rev. B* **70**, 245113 (2004).
  - [13] G. Chen, H.-Y. Kee, and Y. B. Kim, *Phys. Rev. Lett.* **113**, 197202 (2014).
  - [14] L. N. Bulaeviskii, C. D. Batista, M. V. Mostovoy, and D. I. Khomskii, *Phys. Rev. B* **78**, 024402 (2008).
  - [15] D. I. Khomskii, *J. Phys.: Condens. Matter* **22**, 164209 (2010).
  - [16] Y. Kamiya and C. D. Batista, *Phys. Rev. Lett.* **108**, 097202 (2012).
  - [17] H. Katsura, N. Nagaosa, and A. V. Balatsky, *Phys. Rev. Lett.* **95**, 057205 (2005).
  - [18] H. Katsura, A. V. Balatsky, and N. Nagaosa, *Phys. Rev. Lett.* **98**, 027203 (2007).
  - [19] A. Bolens, *Phys. Rev. B* **98**, 125135 (2018).
  - [20] A. Bolens, H. Katsura, M. Ogata, and S. Miyashita, *Phys. Rev. B* **97**, 161108(R) (2018).
  - [21] Z. Wang, S. Reschke, D. Hüvonen, S.-H. Do, K.-Y. Choi, M. Gensch, U. Nagel, T. Röm, and A. Loidl, *Phys. Rev. Lett.* **119**, 227202 (2017).
  - [22] A. Little, L. Wu, P. Lampen-Kelley, A. Banerjee, S. Patankar, D. Rees, C. A. Bridges, J.-Q. Yan, D. Mandrus, S. E. Nagler, and J. Orenstein, *Phys. Rev. Lett.* **119**, 227201 (2017).
  - [23] S. Reschke, F. Mayr, S. Widmann, H.-A. K. von Nidda, V. Tsurkan, M. V. Eremin, S.-H. Do, K.-Y. Choi, Z. Wang, and A. Loidl, *J. Phys.: Condens. Matter* **30**, 475604 (2018).
  - [24] C. Wellm, J. Zeisner, A. Alfonsov, A. U. B. Wolter, M. Roslova, A. Isaeva, T. Doert, M. Vojta, B. Büchner, and V. Kataev, *Phys. Rev. B* **98**, 184408 (2018).
  - [25] L. Y. Shi, Y. Q. Liu, T. Lin, M. Y. Zhang, S. J. Zhang, L. Wang, Y. G. Shi, T. Dong, and N. L. Wang, *Phys. Rev. B* **98**, 094414 (2018).
  - [26] M. Barkeshli, E. Berg, and S. Kivelson, *Science* **346**, 722 (2014).
  - [27] D. Aasen, R. S. K. Mong, B. M. Hunt, D. Mandrus, and J. Alicea, *Phys. Rev. X* **10**, 031014 (2020).
  - [28] R. Chari, R. Moessner, and J. G. Rau, *Phys. Rev. B* **103**, 134444 (2021).
  - [29] K. W. Plumb, J. P. Clancy, L. J. Sandilands, V. V. Shankar, Y. F. Hu, K. S. Burch, H.-Y. Kee, and Y.-J. Kim, *Phys. Rev. B* **90**, 041112(R) (2014).
  - [30] X. Zhou, H. Li, J. A. Waugh, S. Parham, H.-S. Kim, J. A. Sears, A. Gomes, H.-Y. Kee, Y.-J. Kim, and D. S. Dessau, *Phys. Rev. B* **94**, 161106(R) (2016).
  - [31] L. J. Sandilands, Y. Tian, A. A. Reijnders, H.-S. Kim, K. W. Plumb, Y.-J. Kim, H.-Y. Kee, and K. S. Burch, *Phys. Rev. B* **93**, 075144 (2016).
  - [32] S. M. Winter, Y. Li, H. O. Jeschke, and R. Valentí, *Phys. Rev. B* **93**, 214431 (2016).
  - [33] W. Wang, Z.-Y. Dong, S.-L. Yu, and J.-X. Li, *Phys. Rev. B* **96**, 115103 (2017).
  - [34] J. Nasu, J. Knolle, D. L. Kovrizhin, Y. Motome, and R. Moessner, *Nat. Phys.* **12**, 912 (2016).
  - [35] A. Banerjee, J. Yan, J. Knolle, C. A. Bridges, M. B. Stone, M. D. Lumsden, D. G. Mandrus, D. A. Tennant, R. Moessner, and S. E. Nagler, *Science* **356**, 1055 (2017).
  - [36] A. Banerjee, C. A. Bridges, J. Q. Yan, A. A. Aczel, L. Li, M. B. Stone, G. E. Granroth, M. D. Lumsden, Y. Yiu, J. Knolle, S. Bhattacharjee, D. L. Kovrizhin, R. Moessner, D. A. Tennant, D. G. Mandrus, and S. E. Nagler, *Nat. Mater.* **15**, 733 (2016).
  - [37] Y. Kasahara, T. Ohnishi, Y. Mizukami, O. Tanaka, S. Ma, K. Sugii, N. Kurita, H. Tanaka, J. Nasu, Y. Motome, T. Shibauchi, and Y. Matsuda, *Nature* **559**, 227 (2018).
  - [38] T. Yokoi, S. Ma, Y. Kasahara, S. Kasahara, T. Shibauchi, N. Kurita, H. Tanaka, J. Nasu, Y. Motome, C. Hickey, S. Trebst, and Y. Matsuda, *Science* **373**, 568 (2021).
  - [39] N. Janša, A. Zorko, M. Gomilšek, M. Pregelj, K. W. Krämer, D. Biner, A. Biffin, C. Rüegg, and M. Klanjšek, *Nat. Phys.* **14**, 786 (2018).
  - [40] S.-H. Do, S.-Y. Park, J. Yoshitake, J. Nasu, Y. Motome, Y. S. Kwon, D. T. Adroja, D. J. Voneshen, K. Kim, T. H. Jang, J. H. Park, K.-Y. Choi, and S. Ji, *Nat. Phys.* **13**, 1079 (2017).

- [41] S. Widmann, V. Tsurkan, D. A. Prishchenko, V. G. Mazurenko, A. A. Tsirlin, and A. Loidl, *Phys. Rev. B* **99**, 094415 (2019).
- [42] Y. Kubota, H. Tanaka, T. Ono, Y. Narumi, and K. Kindo, *Phys. Rev. B* **91**, 094422 (2015).
- [43] S. Y. Park, S. H. Do, K. Y. Choi, D. Jang, T. H. Jang, J. Schefer, C. M. Wu, J. S. Gardner, J. M. S. Park, J. H. Park, and S. Ji, [arXiv:1609.05690](https://arxiv.org/abs/1609.05690).
- [44] M. He, X. Wang, L. Wang, F. Hardy, T. Wolf, P. Adelman, T. Brückel, Y. Su, and C. Meingast, *J. Phys.: Condens. Matter* **30**, 385702 (2018).
- [45] X. Mi, X. Wang, H. Gui, M. Pi, T. Zheng, K. Yang, Y. Gan, P. Wang, A. Li, A. Wang, L. Zhang, Y. Su, Y. Chai, and M. He, *Phys. Rev. B* **103**, 174413 (2021).
- [46] P. A. Franken, A. E. Hill, C. W. Peters, and G. Weinreich, *Phys. Rev. Lett.* **7**, 118 (1961).
- [47] S. A. Denev, T. T. A. Lummen, E. Barnes, A. Kumar, and V. Gopalan, *J. Am. Ceram. Soc.* **94**, 2699 (2011).
- [48] E. V. Stroganov and K. V. Ovchinnikov, *Ser. Fiz. Khim.* **12**, 152 (1957).
- [49] M. Ziatdinov, A. Banerjee, A. Maksov, T. Berlijn, W. Zhou, H. B. Cao, J.-Q. Yan, C. A. Bridges, D. G. Mandrus, S. E. Nagler, A. P. Baddorf, and S. V. Kalinin, *Nat. Commun.* **7**, 13774 (2016).
- [50] H. B. Cao, A. Banerjee, J.-Q. Yan, C. A. Bridges, M. D. Lumsden, D. G. Mandrus, D. A. Tennant, B. C. Chakoumakos, and S. E. Nagler, *Phys. Rev. B* **93**, 134423 (2016).
- [51] R. D. Johnson, S. C. Williams, A. A. Haghighirad, J. Singleton, V. Zapf, P. Manuel, I. I. Mazin, Y. Li, H. O. Jeschke, R. Valentí, and R. Coldea, *Phys. Rev. B* **92**, 235119 (2015).
- [52] A. Banerjee, P. Lampen-Kelley, J. Knolle, C. Balz, A. A. Aczel, B. Winn, Y. Liu, D. Pajerowski, J. Yan, C. A. Bridges, A. T. Savici, B. C. Chakoumakos, M. D. Lumsden, D. A. Tennant, R. Moessner, D. G. Mandrus, and S. E. Nagler, *npj Quantum Mater.* **3**, 8 (2018).
- [53] C. Balz, L. Janssen, P. Lampen-Kelley, A. Banerjee, Y. H. Liu, J.-Q. Yan, D. G. Mandrus, M. Vojta, and S. E. Nagler, *Phys. Rev. B* **103**, 174417 (2021).
- [54] S. Mu, K. D. Dixit, X. Wang, D. L. Abernathy, H. Cao, S. E. Nagler, J. Yan, P. Lampen-Kelley, D. Mandrus, C. A. Polanco, L. Liang, G. B. Halász, Y. Cheng, A. Banerjee, and T. Berlijn, *Phys. Rev. Research* **4**, 013067 (2022).
- [55] L. Wu, A. Little, E. E. Aldape, D. Rees, E. Thewalt, P. Lampen-Kelley, A. Banerjee, C. A. Bridges, J.-Q. Yan, D. Boone, S. Patankar, D. Goldhaber-Gordon, D. Mandrus, S. E. Nagler, E. Altman, and J. Orenstein, *Phys. Rev. B* **98**, 094425 (2018).
- [56] P. Lampen-Kelley, S. Rachel, J. Reuther, J.-Q. Yan, A. Banerjee, C. A. Bridges, H. B. Cao, S. E. Nagler, and D. Mandrus, *Phys. Rev. B* **98**, 100403(R) (2018).
- [57] J. Nasu, M. Udagawa, and Y. Motome, *Phys. Rev. Lett.* **113**, 197205 (2014).
- [58] J. Nasu, M. Udagawa, and Y. Motome, *Phys. Rev. B* **92**, 115122 (2015).
- [59] A. M. Samarakoon, G. Wachtel, Y. Yamaji, D. A. Tennant, C. D. Batista, and Y. B. Kim, *Phys. Rev. B* **98**, 045121 (2018).
- [60] A. Catuneanu, Y. Yamaji, G. Wachtel, Y. B. Kim, and H.-Y. Kee, *npj Quantum Mater.* **3**, 23 (2018).
- [61] H. Li, H.-K. Zhang, J. Wang, H.-Q. Wu, Y. Gao, D.-W. Qu, Z.-X. Liu, S.-S. Gong, and W. Li, *Nat. Commun.* **12**, 4007 (2021).
- [62] P. Lunkenheimer, J. Müller, S. Krohns, F. Schrettle, A. Loidl, B. Hartmann, R. Rommel, M. de Souza, C. Hotta, J. A. Schlueter, and M. Lang, *Nat. Mater.* **11**, 755 (2012).
- [63] E. Gati, J. K. H. Fischer, P. Lunkenheimer, D. Zielke, S. Köhler, F. Kolb, H.-A. K. von Nidda, S. M. Winter, H. Schubert, J. A. Schlueter, H. O. Jeschke, R. Valentí, and M. Lang, *Phys. Rev. Lett.* **120**, 247601 (2018).
- [64] S. Iguchi, S. Sasaki, N. Yoneyama, H. Taniguchi, T. Nishizaki, and T. Sasaki, *Phys. Rev. B* **87**, 075107 (2013).
- [65] D. V. Efremov, J. van den Brink, and D. I. Khomskii, *Nat. Mater.* **3**, 853 (2004).
- [66] J. van den Brink and D. I. Khomskii, *J. Phys.: Condens. Matter* **20**, 434217 (2008).
- [67] H. Li, T. T. Zhang, A. Said, G. Fabbris, D. G. Mazzone, J. Q. Yan, D. Mandrus, G. B. Halász, S. Okamoto, S. Murakami, M. P. M. Dean, H. N. Lee, and H. Miao, *Nat. Commun.* **12**, 3513 (2021).